ZnO/MoO_3 Heterojunction thick films to detect ppb level Volatile Organic Compounds

Sai Kiran Ayyala, and James A. Covington, *Member, IEEE*

***Abstract*— The development of a fast, stable metal oxide-based VOC sensor for the detection of trace level ppb concentrations, remains a challenge. Recently, many composite materials have been investigated to try and develop sensors with these characteristics. Here, we report on the development of ZnO/MoO_3 heterojunction thick film devices, fabricated by a spin-coating technique, to detect a wide range of VOCs at application relevant ppb level concentrations. For comparison, pristine ZnO and pristine MoO_3 devices were also fabricated. Sensors were tested at different temperatures and resulting in an optimum temperature of 380°C. The sensors were tested towards 11 different VOCs at ppb concentrations. Of all the sensors tested, the heterojunction devices showed the highest response to VOCs, with highest sensitivity towards 200 ppb of ethanol. The results compared well with the pristine materials, with the response of the ZnO material being 6 times smaller and MO_3 10 times smaller compared to the heterojunction sensors. The response times of the heterojunction devices was also faster, at around 30 sec for ethanol compared with 120 sec for pristine materials.**

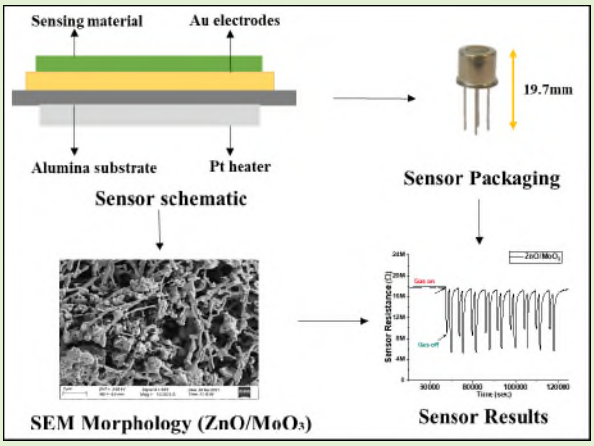

***Index Terms*— Gas sensors; Metal oxides; Heterojunctions; Volatile Organic Compounds; ppb detection**

I. Introduction

Over the past decade, the number of toxic chemicals in our air has been steadily rising [1, 2]. Many VOCs pose a health risk even at very low concentrations (from a few parts per billion) if exposed for longer durations [3]. Therefore, detection of these toxic VOCs at concentrations in ppb (parts-per-billion) has become ever more important. Compared to other conventional gas detection approaches, metal oxide (MOX) based gas sensors have been acknowledged as a cost-effective yet efficient method to detect VOCs [4, 5]. However, detecting trace level VOCs has always been a challenge. There have been several strategies proposed to enhance the sensitivity of metal oxide semiconductor gas sensors. Over the last decade, *n-p* and *n-n* heterojunction composite materials have attracted the wide attention of many researchers [6]. Geometrically, heterojunction gas sensors consist of two different metal oxides that function together as the sensing material. This may overcome some of the existing inherent problems of monolithic gas sensors, as the hetero contacts enable the electron transfer between two different materials with tuneable bandgap, which can improve the overall detection mechanism making it a promising approach to detect VOCs even at trace concentrations [7].

This paper was submitted for review on 26th February 2022.

Sai Kiran Ayyala (SKA), and James A Covington (JAC) are affiliated with the School of Engineering, University of Warwick, Coventry, CV4 7AL, United Kingdom (e-mail: SKA: sai-kiran.ayyala@warwick.ac.uk and JAC: J.A.Covington@warwick.ac.uk)

Molybdenum trioxide (MoO_3) is an *n*-type material with a tuneable bandgap of 2.8 - 3.6eV, high electron mobility and unique layered structure, promoting it as interesting material for gas sensing [8]. ZnO is a second *n*-type material has been previously explored, due to its low electrical resistivity and high response towards many gases and VOCs. Although pure MoO_3 sensors has been previously investigated, the very high intrinsic resistivity and poor sensor performance has limited the use of this material [9]. However, the combination of an *n-n* heterojunction can lead to a synergy effect, which can enhance the overall gas sensing performance [10].

There are many previously reported heterojunction devices tested towards VOCs. For example, α-MoO_3-ZnO *n-n* heterojunction composites were developed and tested towards 100 ppm ethanol with a sensor response (R_a/R_g = 11) [11]. MoO_3/TiO_2 core-shell *p-n* heterojunction was tested towards 10ppm of ethanol with low sensor response (R_g/R_a = 5) [12]. Different percentages of ZnO was incorporated into MoO_3 by Navas et.al and tested towards 500 ppm ethanol (R_g/R_a= 175) [13]. Dayan et.al. developed a thick film ZnO:MoO_3 heterojunction sensor, but only tested the device to hydrogen gas [14]. Though the sensor responses for these gas sensors was relatively high, they all were fabricated using hydrothermal deposition techniques and were tested only to

selective VOCs in the parts-per-million concentration range (ppm). Anupriya et.al. developed a thick film device with a 50:50 weight ratio of WO_3-ZnO using a screen-printing technique. However, these *n-n* heterojunction sensors were only tested towards NO_2 (100ppb - 800ppb, R_a/R_g = 160) and ethanol (5 – 100 ppm, R_a/R_g = 38) [15]. They attribute the equal mole fraction of both the metal oxides as a contributing factor to this enhanced sensitivity.

To the best of our knowledge, the development of ZnO/MoO_3 heterojunction thick films by spin-coating method and their testing to a wide variety of VOCs at ppb concentrations have not been reported in the literature. In this work, we have fabricated two different *n*-type metal oxides as an *n-n* heterojunction using photolithography assisted spin-coating technique. For comparison purposes, pristine ZnO and pristine MoO_3 thick films were also fabricated in the same method, and all the sensors are tested to ppb level concentrations of 11 different VOCs.

A. Sensor Fabrication

Alumina substrate (2mm x 2mm), with screen printed gold electrodes on top and platinum heater at the bottom, were used for all the sensors. Pristine ZnO, pristine MoO_3 and ZnO/MoO_3 heterojunction metal oxides were deposited using a photolithography assisted spin-coating technique [16]. ZnO (99.99% trace metal basis) and MoO_3 (99.99% trace metal basis) were purchased from Sigma Aldrich. Spin coating ink was formulated by mixing 5gm of ZnO powder and 5g of MoO_3 powder with a 1:1 weight ratio along with 25ml of dirasol-916 (negative photoresist, purchased from Sigma Aldrich) for ZnO/MoO_3 heterojunction films. 10 g of ZnO powder and 10 gm of MoO_3 powder were mixed with 20ml of dirasol-916 ink separately to deposit pristine ZnO and pristine MoO_3 films. 10 ml of de-ionised (DI) water was added to each of these pristine metal oxide mixtures to make it viscous and homogeneous. Substrates were washed thoroughly in a sequential decontamination process using Acetone, iso propanol (IPA), de-ionised (DI) water and dried at room temperature. The formulated ink was then poured onto the substrate and after process optimisation, spun at 3000 RPM for 60 sec on the spin coater (G3P-8, Specialty Coating Systems, USA) with a ramp-up and ramp-down speed of 500 RPM for 10 sec in order to achieve a uniform film. Substrates were exposed to UV light for 5 min to keep the exposed area intact and wash away the unexposed area with DI water. Deposited films were post baked at 80°C until dry and the whole deposition process was repeated multiple times to increase the sensing layer thickness. Finally, all the sensors were fired at 600°C for 2 hours with a temperature ramp of 5°C per minute.

B. Structural Characterisation

The sample's surface morphology cross-section was carried on a scanning electron microscope (SEM) at an accelerating voltage of 3kV. Energy-dispersity X-ray (EDX) spectrometry was carried out separately to understand the composition of the deposited metal oxides. A Bruker D8 Discover powder X-ray diffraction (XRD) instrument was used with Cu Kα X-ray radiation source and Panalytical High score and Plus V4.8 software to match the XRD peaks with the latest ICDD database. X-ray photoelectron spectroscopy (XPS) using Omicron Multiprobe at the Photoemission Research Technology Platform, University of Warwick, was employed to examine the oxidation states present in the metal oxides. The samples were illuminated with an XM1000 monochromatic Al Kα X-ray source (hv = 1486.7 eV). The produced data were analysed with the CasaXPS package, using Shirley backgrounds and mixed Gaussian-Lorentzian (Voigt) lineshapes.

C. Gas Testing

All the sensors are tested towards different VOCs at the given concentrations as shown in TABLE 1. The respective ppb concentrations were achieved using a diffusion setup. The flow over the sensors was controlled using 2 mass flow controllers (MFCs) capable of supplying 500 ml/min. Both the gases lines were connected to a zero-air line and are allowed to flow through 2 molecular sieves (120 ml, type 5A) before the MFCs. Here one line runs through the headspace vials and the other runs directly to the sensor holder. The sensors were placed in a chamber and measured using the AS-330 Sensor management system (Atmospheric Sensor Ltd, UK). The system is controlled by software that allows setting the desired input parameters, including heater temperature, heater resistance and duration of the gas purge and gives the output data including the actual operating temperature and sensor resistance etc. The ppb concentrations emanating from the diffusion set up for each of the VOCs are calibrated using a commercial PID (Photo-Ionization Detector) from Ion Science, UK (Tiger).

TABLE I
TARGET GASES WITH THE RESPECTIVE CONCENTRATIONS TESTED IN THIS EXPERIMENT

VOC Gas	Concentrations
Acetone(C_3H_6O)	200 – 800 ppb
Ethanol (C_2H_5OH)	200 – 800 ppb
Methanol (CH_3OH)	200 – 800 ppb
Propanol-2 (C_3H_8O)	200 – 800 ppb
Toluene (C_7H_8)	200 – 800 ppb
Hexane (C_6H_{14})	200 – 950 ppb
Xylene-p ($C_6H_4(CH_3)_2$	200 – 800 ppb
Ethylbenzene ($C_6H_5C_2H_5$)	200 – 800 ppb
Isoprene (C_5H_8)	50 – 500 ppb
Butyric acid ($C_4H_8O_2$)	200 – 800 ppb
Isobutylene (C_4H_8)	1 ppm and 5 ppm

In our experiments, zero air was used as the carrier gas and the respective VOCs at the given concentrations are the target gas.

The gas response is defined as the ratio of sensor resistance in zero air (R_a) to the sensor resistance in the target gas (R_g).

II. Results and Discussion

A. SEM

Topographical and cross-sectional images of the samples are given in Fig. 1. SEM image Fig. 1 (a). confirms that the ZnO particles are formed like micro-granules (1-2 µm in diameter) with a material thickness around 35 µm (± 0.3 µm) (Fig. 1 (b)) measured at 2 different points. MoO_3 in Fig. 1(c). looks like micro-grass with the size of the needles around 8-10 µm in length and 1 µm in diameter and the deposited film thickness of 47 µm (± 0.2 µm) (Fig. 1(d)) taken at 2 different points. ZnO/MoO_3 heterojunction film shown in Fig. 1 (e) depicts the morphology of ZnO micro-granules decorated on the surface of the MoO_3 micro-needles making the film thickness around 40 µm (± 1 µm) (Fig. 1 (f)) taken from 2 different places. Interestingly, heterojunction material is more porous than the pristine samples and so were expected to have a higher surface to volume ratio, potentially offering higher adsorption rates. These topographical characteristics are optimal for the detection of gases even at trace concentrations.

(a) (b)

(c) (d)

(e) (f)

Fig. 1. Scanning Electron Microscope images of (a) ZnO topography, (b) ZnO cross-section, (c) MoO_3 topography, (d) MoO_3 cross-section, (e) ZnO/MoO_3 topography, and (f) ZnO/MoO_3 cross-section

B. EDX

Energy-dispersive X-ray (EDX) analysis was carried out to report the elemental composition of ZnO, MoO_3 and ZnO/MoO_3 films, as shown in Fig. 2 (a), (b) and (c), respectively. The ratio of atomic percentages of Zn (53.95%) and O (46.05%) is 1:1 for ZnO film and Mo (25%) and O (75%) is 1:3 for MoO_3 samples. The EDX spectra confirm the Zn (20.72%), Mo (21.24%), and O (57.86%) elements corresponding to ZnO and MoO_3 metal-oxide presence in ZnO/MoO_3 heterojunction film.

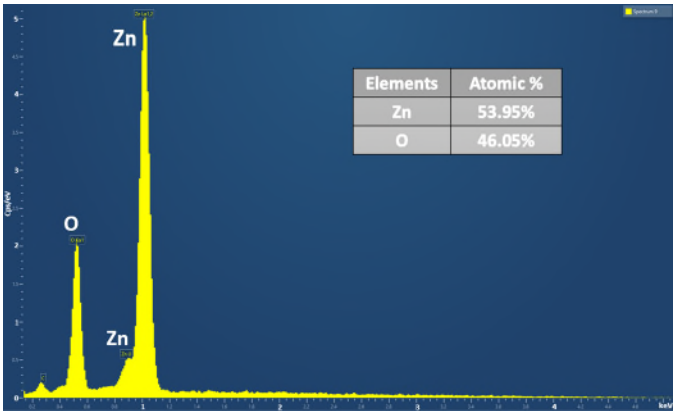

(a)

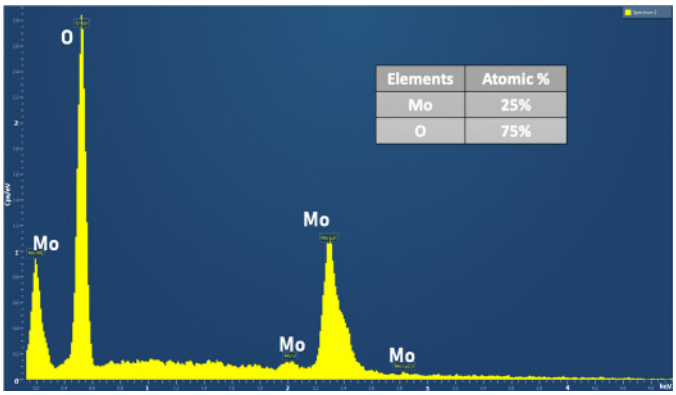

(b)

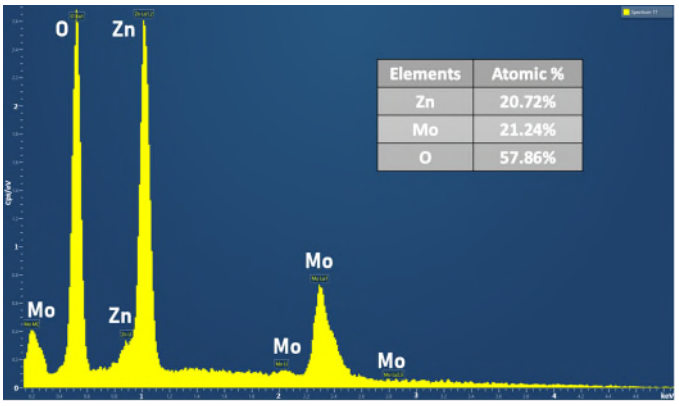

(c)

Fig. 2. EDX energy-dispersive patterns of (A) ZnO, (B) MoO_3, and (C) ZnO/MoO_3

C. XRD

The crystal structure of pristine ZnO, pristine MoO_3 and ZnO/MoO_3 heterojunction are confirmed using XRD measurements. The XRD analysis was carried out on the annealed samples of the respective metal oxides, deposited on alumina substrates separately. The diffraction peaks of pristine

ZnO in Fig. 3 (a) shows the formation of a wurtzite type hexagonal crystal system with a space group: P63mc (IDCC file no. 04-003-2106) with cell parameters at (Å): 3.2501, b (Å): 3.2501, c (Å): 5.2071, as observed at [17]. The diffraction peaks from pristine MoO_3 given in Fig. 3 (b) confirms orthorhombic crystal structure with space group: Pbnm, with cell parameters of a (Å): 3.9616, b (Å): 13.8560, c (Å): 3.6978 referred to the IDCC file no. 04-012-8070 [18]. As shown in Fig. 3 (c), the XRD data of the ZnO/MoO_3 heterojunction shows mixed peaks from hexagonal ZnO, orthorhombic MoO_3, and certain peaks of consists of Zn/MoO_4(*). The heterojunction film has a formation of triclinic type anorthic crystal structure with cell parameters a (Å): 6.9650, b (Å): 8.3690, c (Å): 9.6930 with an IDCC reference code: 04-018-2283 having cell volume of 519.91 (106 pm3) and space group: P-1 [19]. However, the presence of ZnO and MoO_3 peaks validates the formation of the ZnO/MoO_3 composite. The XRD stick pattern of the standard metal oxides as per the latest IDCC files are given below each plot for reference.

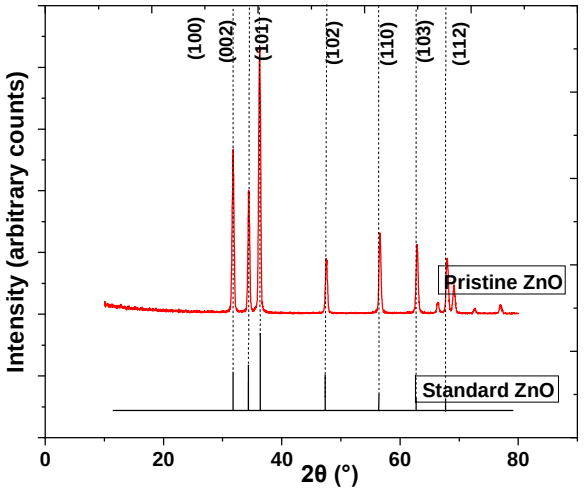

(a)

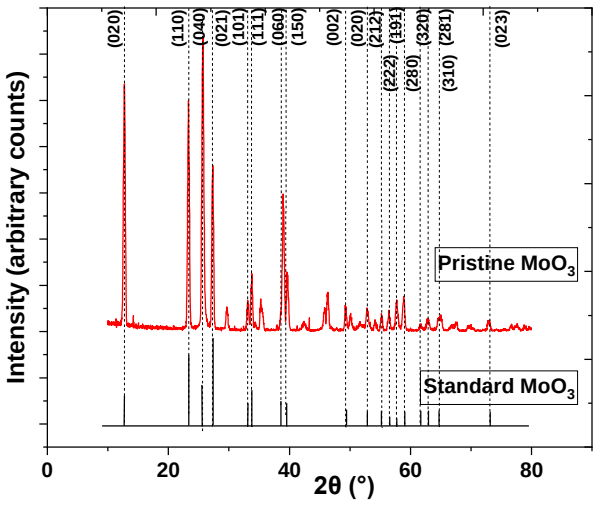

(b)

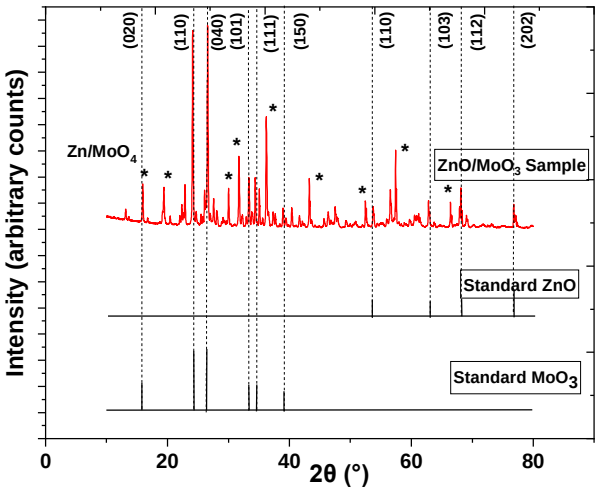

(c)

Fig. 3. XRD diffraction patterns of (a) ZnO, (b) MoO_3, and (c) ZnO/MoO_3

D. XPS

The valance states and oxidation numbers of the predominant elements present in the ZnO/MoO_3 heterojunction metal oxide film were elucidated by XPS analysis. The measurements were conducted at room temperature and a take-off angle of 90° with respect to the sample surface. The spectrometer binding energy scale was calibrated using the Fermi edge of a polycrystalline Ag sample, measured immediately before commencing the measurements. The deconvoluted Mo 3d5/2, Zn 2p3/2, O 1S, and C 1S spectrum are shown in Fig. 4 (a), (b), (c) and (d), respectively. ZnO peaks from the Zn 2p3/2 region were observed at 1021.48eV. There are different oxidation states of Mo observed from the heterojunction sample. The bonding peaks corresponding to Mo (+6) states are observed at 234.01 eV, Mo (+5) are observed at 236 eV, and Mo (+4) are observed at binding energy 231.95 eV, as previously observed at [6, 19, 20]. ZnO was observed at the Zn 2p3/2 region as shown previously at [22]. From the O 1S orbital, Zn oxide was observed at 529.77 eV and Mo oxide was observed at 530.37 eV. There are other peaks observed due to the atmospheric oxygen present on the heterojunction film as mentioned in the plot. The C-C/C-H, C-O, C=O, and O=C-O peaks are observed in the C 1S region at 285 eV, 286.38 eV, 287.57 eV, and 289.16 eV, respectively. To prevent the surface from becoming positively charged during the experiment, a CN10 electron flood gun was used to neutralise the surface and the spectra subsequently referenced to the C-C/C-H component of the C 1s region at 285.0 eV. The appearance of ZnO and MoO_3 from the XPS survey spectrum (not shown here) confirms the successful formation of ZnO and MoO_3 composite that is consistent with elemental mapping.

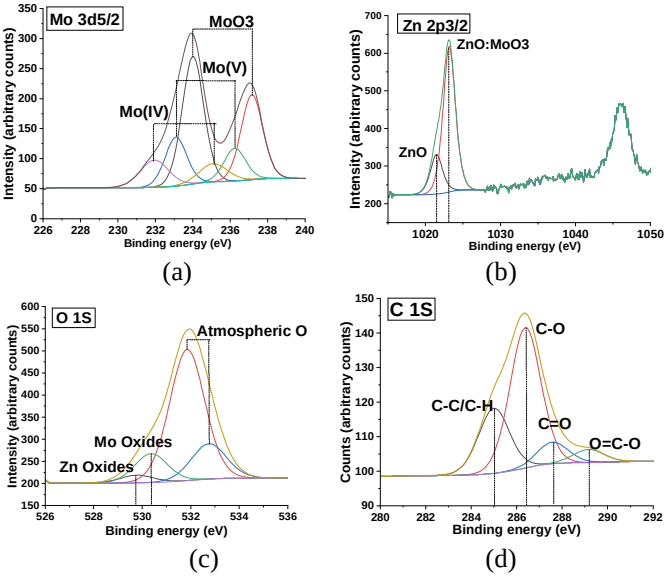

Fig 4. XPS patterns of ZnO/MoO_3 heterojunctions film (a) Mo 3d5/2, (b) Zn 2p3/2, (c) O 1s, and (d) C 1S.

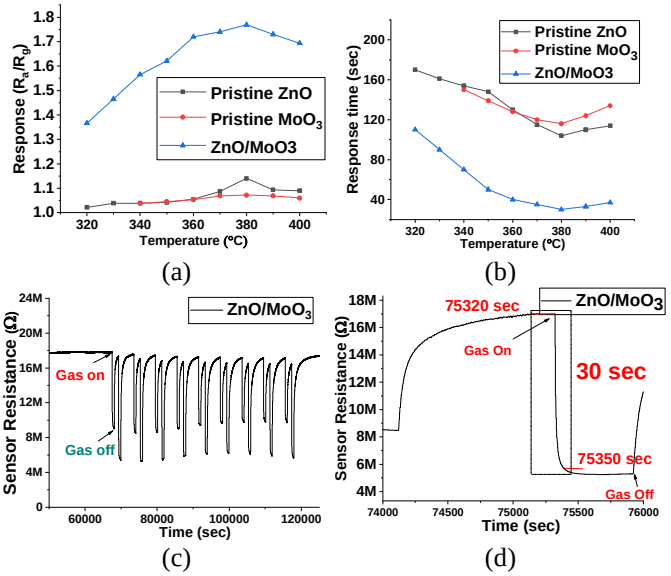

Fig. 5. (a) Temperature(°C) versus Response (R_a/R_g) of all the devices, (b) Temperature (°C) versus response time (sec) of all the devices, (c) Sensitivity graph of ZnO/MoO_3 heterojunction device towards 1ppm and 5ppm Isobutylene gas at 380°C, (d) Response time of ZnO/MoO_3 device for one cycle

E. Gas Testing

The detection mechanism of MOX based gas sensor is chemo-resistive i.e., the chemisorption/physisorption of gas/vapour molecules onto the sensing surface, which leads to a change in the electrical resistance [23]. Generally, the sensors operating temperature plays a vital role in the sensitivity and response time of the sensors. Thus initially, ZnO/MoO_3 sensors were tested at different heater temperatures from 50°C to 400°C towards 1ppm isobutylene (ISB) gas in dry air. In addition, pristine ZnO and pristine MoO_3 based devices were also tested over this temperature range, towards the same gas concentration, to understand the optimum operating temperature for all the sensors. As shown in Fig. 5 (a), (b), ZnO/MoO3, pristine ZnO, pristine MoO3 sensors responded maximum towards ISB at 380°C with a relative response R_a/R_g = 1.8, 1.14, and 1.07 for 1 ppm ISB, respectively. The response times for all the gas sensors was quicker at 380°C than the rest of the temperatures, with the response time less than 30 sec for ZnO/MoO_3 sensor (Fig. 5 (d)). However, the relative response and response time was better for ZnO/MoO_3 devices than the pristine oxides. Furthermore, sensor stability and repeatability are also important factors to qualify a good gas sensor. Therefore, the ZnO/MoO_3 sensor was tested repeatedly at 1 ppm and 5 ppm of ISB gas. As shown in Fig. 5 (c), the baseline resistance decreases when VOC gas (reducing gas) molecules interact with an n-type sensing material (*n-n* heterojunction as in this case). The repeatedly stable responses demonstrate that ZnO/MoO_3 is a good choice for heterojunction gas sensors.

The heterojunction sensors, along with pristine metal oxides, were tested on all the other VOCs at ppb level concentrations at the same operating temperature. Here the vapours tested were acetone, ethanol, methanol, hexane, propanol-2, toluene, butyric acid, ethylbenzene, xylene, and isoprene. Fig. 6 (a) illustrates the relative response (R_a/R_g) versus ppb concentrations for all the sensors for the respective target vapours. The heterojunction sensors responded better than the pristine sensors towards all the vapours. This enhanced performance could be attributed to the formation of ZnO and MoO_3 heterojunction composite leading to the synergy effect commonly known as the spill-over. In this effect, a target gas molecule interacts with one *n*-type material, which releases secondary by-products. These by-products undergo adsorption on the other n-type material and directly affects the sensing performance. Secondly, as the two different materials have different energy band gaps, electron transfer occurs from higher-energy conduction band to low-energy conduction band until the Fermi levels of both the materials are equilibrated at the interface of the *n-n* junction. Thus, resulting in an 'accumulation layer', rather than a depletion layer [23, 24]. This electron transfer phenomenon leads to band bending, which further enhances the oxygen adsorption rate. Thirdly, the heterojunction films have a higher porosity, as seen in Fig. 1 (e), helps the gas molecules to penetrate further and improves the rate of target gas reaction at the active surface sites throughout the thick film.

The overall performance of the pristine MoO_3 oxides was poor compared to the other thick films due to their high intrinsic resistivity, as shown in Fig. 6 (c), (d). However, the response was particularly significant towards ethanol and methanol vapours over the other VOCs. The heterojunction sensor resistance did not saturate upon target gas introduction due to the leakage of gas from the diffusion setup. Therefore, we see a steady slope of resistance at each concentration. The sensors

response (R_a/R_g) for 200 ppb ethanol and methanol vapours were 12.84 and 9.27, respectively (Fig. 6 (b)).

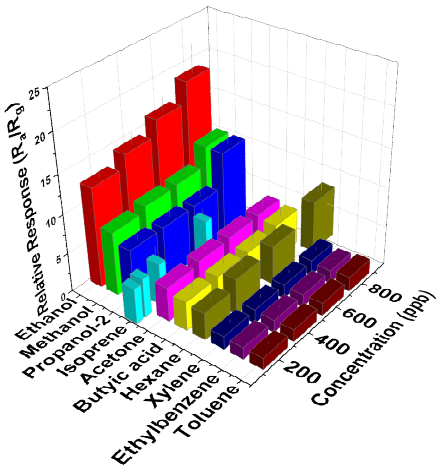

(a)

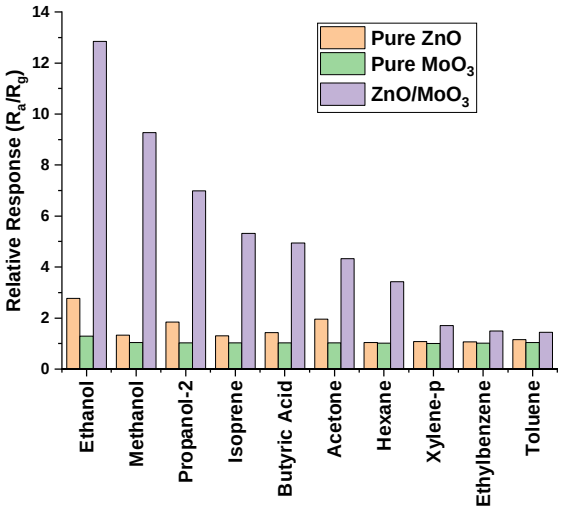

(b)

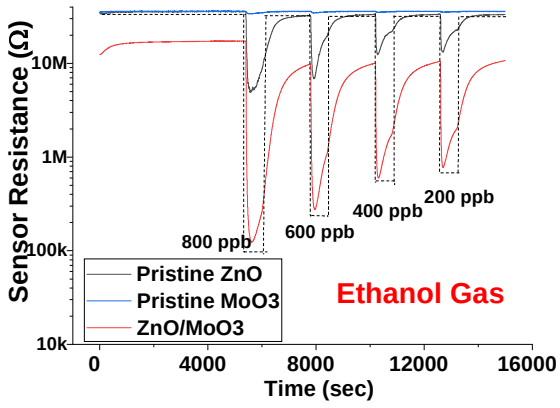

(c)

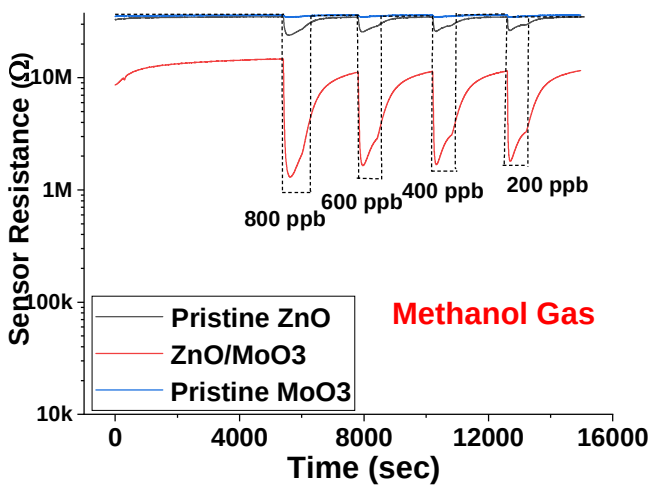

(d)

Fig. 6. (a) Relative responses (Ra/Rg) for all the VOC gases at respective concentrations for ZnO/MoO_3 device, (B) Relative response (Ra/Rg) of all the VOCs at 200ppb concentrations, (C) Sensitivity graph of ZnO/MoO_3 device towards Ethanol vapour, (D) Sensitivity graph of ZnO/MoO_3 device towards methanol vapour.

F. Gas Sensing Mechanism

It is widely believed that the gas sensing mechanism of a metal oxide gas sensor is dependent on surface charge reactions. The chemisorbed atmospheric oxygen ions are present on the surface of the metal oxides in the form of peroxides and super-oxides (O-, O_2^-, O^{2-}) based on the operating temperature where a thin depletion layer is formed [14].

When reducing gas molecules react with this electron-rich *n*-type semiconductor material, the conductance increases, or resistance decreases (as in this case) due to the transfer of charge carriers. When the VOC molecules are oxidised on the surface-adsorbed oxygen species, electrons get released into the conduction band of the sensing material. When this phenomenon takes place, the chemisorbed oxygen species exit the surface of the active layer and free electrons are put back, thereby decreasing the surface conductivity. Therefore, a higher response is seen at higher gas concentrations, as more electrons are generated from the increased gas molecule reaction [26]. Porosity also plays a major role in achieving an enhanced sensitivity of the heterojunction oxides [27]. The SEM images infer that the sensitivity is highly dependent on the porosity of the heterojunction and that the molybdenum component provides a porous substrate for the active zinc component. From the literature, it is evident that the metal oxide packaging structure plays a significant role in gas sensing properties. An equal proportion of the composition of metal oxides in a heterojunction is likely to sit within the packaging structures, which promotes the electron percolation pathways that are more dominated at hetero contacts increasing the contact potential and thus improving the gas response [15]. From EDX results of the heterojunction films, it was confirmed that the presence of equal proportions of Mo and Zn components, which may be an additional factor for this enhanced gas sensitivity.

The charges that existed on the *n-n* heterojunction helps (for example, ethanol or methanol) gas molecules absorb and desorb easily onto the sensing material. In the case of ethanol, the molecules react with oxygen electrons present on the sensing material and escape through CO_2 and H_2O [28]. In the case of methanol, (-OH) it tends to lose hydrogen atoms and pair with oxygen ions present on the active site [29]. One of the possible reactions of ethanol and methanol are given in Eq.1 and Eq.2, respectively.

$$C_2H_5OH + 6O^- \longrightarrow 2CO_2 + 2H_2O + 6e^- \quad \text{(Eq. 1)}$$

$$CH_3OH + O^- \longrightarrow HCHO + H_2O + e^- \quad \text{(Eq. 2)}$$

The tested *n-n* heterojunction ZnO/MoO_3 sensor was showed a higher response and faster detection towards many VOCs over those available in the literature, as shown in TABLE 2.

TABLE 2
COMPARISON OF RELATIVE RESPONSES FOR HETEROJUNCTION OXIDES TOWARDS VOCS

Material	Target gases	Deposition technique	Conc.	Sensitivity (R_a/R_g)	Ref
MoO_3 core-ZnO shell NRs	Ethanol	Hydrothermal	200 ppm	7.62	[9]
α-MoO_3/ZnO Nanosheet	Ethanol	Hydrothermal	100 ppm	10	[11]
WO_3: ZnO	Ethanol	Screen printing	100 ppm	38	[15]
ZnO Nanoparticles	Ethanol	Hydrothermal	100 ppm	7	[28]
G-CuO/ZnO	Ethanol	Hydrothermal	500ppm	16	[28]
MoO_3 Nanosheets	Ethanol	Hydrothermal	100 ppm	15	[30]
Au-MoO_3 Nanocomposites	Ethanol	Hydrothermal	100 ppm	102	[30]
h-MoO_3	Acetone	Hydrothermal	1.2 ppm	1.12	[31]
α-MoO_3/α-Fe_2O_3	Xylene and Methanol	Hydrothermal	100 ppm	6.9 and 3	[32]
MoO_3 Microrods	Ethanol	Hydrothermal	500ppm	8.2	[33]
ZnO/MoO_3 Thick films	Ethanol and methanol	Spin-coating	200ppb	12.84 and 9.27	This work

III. CONCLUSIONS

In this work, we report on the successful development of an n-n heterojunction thick film ZnO/MoO_3, using a spin coating technique and tested it towards 11 different VOCs, in ppb concentrations. We have also fabricated pristine ZnO and pristine MoO_3 devices to compare the performance of the sensors with the heterojunction device. SEM-EDX cross-section images indicate 40µm heterojunction thick films were deposited. EDX confirms the compositions of ZnO and MoO_3 materials in the heterojunction. XRD patterns show the formation of ZnO and MoO_3 composite with an anorthic crystal structure. XPS analysis validates the presence of different oxidation states that are responsible for gas detection in the heterojunction film. Overall, ZnO/MoO_3 heterojunction sensors performed better than the pristine oxides. They were responding maximum at 380°C, with a response time less than 30 sec. Among all the VOCs tested, the response is maximum for ethanol and methanol gases with the relative response (R_a/R_g) 12.84 and 9.7, respectively. This is the highest response observed for a thick-film heterojunction sensor at ppb concentrations making it an excellent alternative for detecting VOCs at trace level ppb concentrations.

REFERENCES

[1] H. Nguyen and S. A. El-Safty, "Meso- and macroporous Co3O4 nanorods for effective VOC gas sensors," *J. Phys. Chem. C*, vol. 115, no. 17, pp. 8466–8474, 2011.

[2] K. Zhang, S. Qin, P. Tang, Y. Feng, and D. Li, "Ultra-sensitive ethanol gas sensors based on nanosheet-assembled hierarchical ZnO-In2O3 heterostructures," *J. Hazard. Mater.*, vol. 391, no. January, p. 122191, 2020.

[3] M. Leidinger, T. Sauerwald, T. Conrad, W. Reimringer, G. Ventura, and A. Schütze, "Selective detection of hazardous indoor VOCs using metal oxide gas sensors," *Procedia Eng.*, vol. 87, pp. 1449–1452, 2014.

[4] J. Wang, Q. Zhou, S. Peng, L. Xu, and W. Zeng, "Volatile Organic Compounds Gas Sensors Based on Molybdenum Oxides: A Mini Review," *Front. Chem.*, vol. 8, no. May, pp. 1–7, 2020.

[5] C. Wang *et al.*, "In-situ generated TiO2/α-Fe2O3 heterojunction arrays for batch manufacturing of conductometric acetone gas sensors," *Sensors Actuators, B Chem.*, vol. 340, no. April, p. 129926, 2021.

[6] J. Li *et al.*, "Synthesis of 1D α-MoO3/0D ZnO heterostructure nanobelts with enhanced gas sensing properties," *J. Alloys Compd.*, vol. 788, pp. 248–256, 2019.

[7] Z. Ling, C. Leach, and R. Freer, "Heterojunction gas sensors for environmental NO2 and CO2 monitoring," *J. Eur. Ceram. Soc.*, vol. 21, no. 10–11, pp. 1977–1980, 2001.

[8] R. Malik, N. Joshi, and V. K. Tomer, " Advances in the designs and mechanisms of MoO 3 nanostructures for gas sensors: a holistic review ," *Mater. Adv.*, vol. 3, pp. 4190–4227, 2021.

[9] W. I. Lee, M. Bonyani, J. K. Lee, C. Lee, and S. B. Choi, "Volatile organic compound sensing properties of MoO3–ZnO core–shell nanorods," *Curr. Appl. Phys.*, vol. 18, pp. S60–S67, 2018.

[10] S. Y. Yi *et al.*, "Morphological Evolution Induced through a Heterojunction of W-Decorated NiO Nanoigloos: Synergistic Effect on High-Performance Gas Sensors," *ACS Appl. Mater. Interfaces*, vol. 11, no. 7, pp. 7529–7538, 2019.

[11] H. L. Yu *et al.*, "Synthesis and H 2S gas sensing properties of cage-like α-MoO 3/ZnO composite," *Sensors Actuators, B Chem.*, vol. 171–172, pp. 679–685, 2012.

[12] Y. J. Chen *et al.*, "α-MoO3/TiO2 core/shell nanorods: Controlled-synthesis and low-temperature gas sensing properties," *Sensors Actuators, B Chem.*, vol. 155, no. 1, pp. 270–277, 2011.

[13] N. Illyaskutty, H. Kohler, T. Trautmann, M. Schwotzer, and V. P. M. Pillai, "Enhanced ethanol sensing response from nanostructured MoO3:ZnO thin films and their mechanism of sensing," *J. Mater. Chem. C*, vol. 1, no. 25, pp. 3976–3984, 2013.

[14] M. Science, "Related content A thick-film hydrogen sensor based on a ZnO : MoO 3 formulation," 1998.

[15] A. J. T. Naik, I. P. Parkin, and R. Binions, "Gas sensing studies of an n-n heterojunction metal oxide semiconductor sensor array based on WO3 and ZnO composites," *Proc. IEEE Sensors*, no. November,

2013.
[16] S. K. Ayyala and J. A. Covington, “Nickel-oxide based thick-film gas sensors for volatile organic compound detection,” *Chemosensors*, vol. 9, no. 9, 2021.
[17] E. H. Kisi and M. M. Elcombe, “u parameters for the wurtzite structure of ZnS and ZnO using powder neutron diffraction,” *Acta Crystallogr. Sect. C Cryst. Struct. Commun.*, vol. 45, no. 12, pp. 1867–1870, 1989.
[18] H. Sitepu, B. H. O’Connor, and D. Li, “Comparative evaluation of the March and generalized spherical harmonic preferred orientation models using X-ray diffraction data for molybdite and calcite powders,” *J. Appl. Crystallogr.*, vol. 38, no. 1, pp. 158–167, 2005.
[19] L. Robertson, M. Duttine, M. Gaudon, and A. Demourgues, “Cobalt-zinc molybdates as new blue pigments involving Co2+ in distorted trigonal bipyramids and octahedra,” *Chem. Mater.*, vol. 23, no. 9, pp. 2419–2427, 2011.
[20] Y. Liu *et al.*, “Synthesis of bio-based methylcyclopentadiene via direct hydrodeoxygenation of 3-methylcyclopent-2-enone derived from cellulose,” *Nat. Commun.*, vol. 12, no. 1, pp. 1–7, 2021.
[21] G. R. Li, Z. L. Wang, F. L. Zheng, Y. N. Ou, and Y. X. Tong, “ZnO@MoO3 core/shell nanocables: Facile electrochemical synthesis and enhanced supercapacitor performances,” *J. Mater. Chem.*, vol. 21, no. 12, pp. 4217–4221, 2011.
[22] R. A. Rakkesh, D. Durgalakshmi, P. Karthe, and S. Balakumar, “Role of interfacial charge transfer process in the graphene-ZnO-MoO3 core-shell nanoassemblies for efficient disinfection of industrial effluents,” *Process. Appl. Ceram.*, vol. 13, no. 4, pp. 376–386, 2019.
[23] A. Mirzaei, S. G. Leonardi, and G. Neri, “Detection of hazardous volatile organic compounds (VOCs) by metal oxide nanostructures-based gas sensors: A review,” *Ceram. Int.*, vol. 42, no. 14, pp. 15119–15141, Nov. 2016.
[24] D. R. Miller, S. A. Akbar, and P. A. Morris, “Nanoscale metal oxide-based heterojunctions for gas sensing: A review,” *Sensors Actuators, B Chem.*, vol. 204, pp. 250–272, 2014.
[25] D. Zappa, V. Galstyan, N. Kaur, H. M. M. Munasinghe Arachchige, O. Sisman, and E. Comini, “‘Metal oxide -based heterostructures for gas sensors’- A review,” *Anal. Chim. Acta*, vol. 1039, pp. 1–23, 2018.
[26] K. Inyawilert, A. Wisitsora-At, A. Tuantranont, P. Singjai, S. Phanichphant, and C. Liewhiran, “Ultra-rapid VOCs sensors based on sparked-In2O3 sensing films,” *Sensors Actuators, B Chem.*, vol. 192, pp. 745–754, 2014.
[27] Y. Gao, Q. Kong, J. Zhang, and G. Xi, “General fabrication and enhanced VOC gas-sensing properties of hierarchically porous metal oxides,” *RSC Adv.*, vol. 7, no. 57, pp. 35897–35904, 2017.
[28] C. Qin, Y. Wang, Y. Gong, Z. Zhang, and J. Cao, “CuO-ZnO hetero-junctions decorated graphitic carbon nitride hybrid nanocomposite: Hydrothermal synthesis and ethanol gas sensing application,” *J. Alloys Compd.*, vol. 770, pp. 972–980, 2019.
[29] W. Tang, “Sensing mechanism of SnO 2 / ZnO nanofibers for CH 3 OH sensors : heterojunction effects,” 2017.
[30] H. Yan, P. Song, S. Zhang, J. Zhang, Z. Yang, and Q. Wang, “Au nanoparticles modified MoO3 nanosheets with their enhanced properties for gas sensing,” *Sensors Actuators, B Chem.*, vol. 236, pp. 201–207, 2016.
[31] G. T. Santos, A. A. Felix, and M. O. Orlandi, “Ultrafast Growth of h-MoO3 Microrods and Its Acetone Sensing Performance,” *Surfaces*, vol. 4, no. 1, pp. 9–16, 2020.
[32] D. Jiang *et al.*, “Xylene gas sensor based on α-MoO3/α-Fe2O3 heterostructure with high response and low operating temperature,” *RSC Adv.*, vol. 5, no. 49, pp. 39442–39448, 2015.
[33] Y. Liu, S. Yang, Y. Lu, N. V. Podval’naya, W. Chen, and G. S. Zakharova, “Hydrothermal synthesis of h-MoO 3 microrods and their gas sensing properties to ethanol,” *Appl. Surf. Sci.*, vol. 359, pp. 114–119, 2015.

Sai Kiran Ayyala received his bachelor’s degree on Nanotechnology from Acharya Nagarjuna University, India in 2015, and the M.Sc. degree in Material Sciences from the Sri Sathya Sai Institute of Higher Learning (Deemed to be University), SSSIHL, Prasanthi Nilayam, Puttaparthi, India, in the year 2017. Now, he is currently pursuing his PhD degree at the School of Engineering, University of Warwick, Coventry, UK. His research interests include the development of metal oxide gas sensors for various toxic gases including volatile organic compounds. He uses different approaches to enhance the sensitivity and performance of MOX gas sensors including the deposition of various thick-film metal oxides, material characterization, and evaluation of gas sensors performance.

James A. Covington is a Professor at the School of Engineering, University of Warwick. He received the B.Eng. degree in electronic engineering from the University of Warwick in 1996 and the PhD degree in 2000. His PhD was on the development of CMOS and SOI CMOS gas sensors for room temperature and high-temperature operation. He was a Research Fellow for both the University of Warwick and the University of Cambridge on the development of gas and chemical sensors. He was appointed as a Lecturer with the School of Engineering, University of Warwick, in 2002, being promoted to Associate Professor in 2006 and is currently a Professor of Electronic Engineering. He heads the Biomedical Sensors Laboratory, School of Engineering. He has authored or co-authored over 150 technical papers and patents. His current research interests focus on the development of micro-analysis systems, electronic noses and artificial olfaction, employing a range of novel sensing materials, device structures, and micro-fabrication methods for applications with the environmental and medical application domains.